CERES_EBAF_Ed2.6r

Data Quality Summary (December 16, 2011)

Investigation: **CERES**
Data Product: **EBAF**

Data Set: **Terra (Instruments: CERES-FM1 or CERES-FM2)**
Aqua (Instruments: CERES-FM3 or CERES-FM4)

Data Set Version: **Edition2.6r**

Subsetting Tool Availability: http://ceres.larc.nasa.gov

The purpose of this document is to inform users of the accuracy of this data product as determined by the CERES Science Team. The document summarizes key validation results, provides cautions where users might easily misinterpret the data, provides links to further information about the data product, algorithms, and accuracy, and gives information about planned data improvements. This document also automates registration in order to keep users informed of new validation results, cautions, or improved data sets as they become available.

This document provides a high-level quality assessment of the CERES Energy Balanced and Filled (EBAF) data product. As such, it represents the minimum information needed by scientists for appropriate and successful use of the data product. For a more thorough description of the methodology used to produce EBAF, please see Loeb et al. (2009). It is strongly suggested that authors, researchers, and reviewers of research papers re-check this document for the latest status before publication of any scientific papers using this data product.

Note to Users:

- **EBAF Ed2.6r corrects a code error in the calculation of global mean quantities in EBAF Ed2.6.**
- **EBAF Ed2.6r also corrects for a drift in clear-sky LW TOA flux starting in 2008 associated with an algorithm error.**
- **For a more detailed discussion, please see Section 5.0 of this document.**

NOTE: To navigate the document, use the Adobe Reader bookmarks view option. Select "View" "Navigation Panels" "Bookmarks".

TABLE OF CONTENTS

Section Page

LIST OF FIGURES

Section Page

LIST OF FIGURES

Section Page

LIST OF TABLES

Section Page

1.0 Introduction

CERES instruments fly on the Terra (descending sun-synchronous orbit with an equator crossing time of 10:30 A.M. local time) and Aqua (ascending sun-synchronous orbit with an equator crossing time of 1:30 P.M. local time) satellites. Each CERES instrument measures filtered radiances in the shortwave (SW; wavelengths between 0.3 and 5 μm), total (TOT; wavelengths between 0.3 and 200 μm), and window (WN; wavelengths between 8 and 12 μm) regions. CERES instruments provide global coverage daily, and monthly mean regional fluxes are based upon complete daily samples over the entire globe.

Despite recent improvements in satellite instrument calibration and the algorithms used to determine SW and LW outgoing top-of-atmosphere (TOA) radiative fluxes, a sizeable imbalance persists in the average global net radiation at the TOA from CERES satellite observations. With the most recent CERES Edition3 Instrument calibration improvements, the SYN1deg_lite_Ed2.6 net imbalance is ~3.6 Wm^{-2}, much larger than the expected observed ocean heating rate ~0.58 Wm^{-2} (Loeb et al., 2011a). This imbalance is problematic in applications that use Earth Radiation Budget (ERB) data for climate model evaluation, estimate the Earth's annual global mean energy budget, and in studies that infer meridional heat transports. *The CERES Energy Balanced and Filled (EBAF) dataset uses an objective constrainment algorithm to adjust SW and LW TOA fluxes within their range of uncertainty to remove the inconsistency between average global net TOA flux and heat storage in the Earth-atmosphere system.*

A second problem users of standard CERES Level-3 data have noted is the occurrence of gaps in monthly mean clear-sky TOA flux maps due to the absence in some regions of cloud-free areas occurring at the CERES footprint scale (~20-km at nadir). As a result, clear-sky maps from CERES SSF1deg_lite_Ed2.6 contain many missing regions. *The problem of gaps in clear-sky TOA flux maps is addressed by inferring clear-sky fluxes from both CERES and Moderate Resolution Imaging Spectrometer (MODIS) measurements to produce a new clear-sky TOA flux climatology that provides TOA fluxes in each region every month.*

We urge users to visit the new CERES Data subsetting/visualization/ordering tool, which provides a vastly improved user interface and a wider range of data formats (e.g., ASCII, netCDF) than is available with the ASDC ordering tool, which is limited to HDF.

http://ceres.larc.nasa.gov

2.0 Description

The CERES EBAF_Ed2.6r product is the culmination of several processing steps, as summarized in Table 2-1. Here we use the latest CERES gains and time-dependent spectral response function values (Thomas et al., 2010, Loeb et al., 2011b). To correct for the imperfect spectral response of the instrument, the filtered radiances are converted to unfiltered SW, LW and WN radiances (Loeb et al. 2001). Since there is no LW channel on CERES, LW daytime radiances are determined from the difference between the TOT and SW channel radiances. Instantaneous TOA radiative fluxes are estimated from unfiltered radiances using empirical angular distribution models (ADMs; Loeb et al. 2003, 2005) for scene types identified using retrievals from MODIS measurements (Minnis et al. 2011). Their accuracy has been evaluated in several articles (Loeb et al., 2006; Loeb et al., 2007; Kato and Loeb, 2005). Monthly mean fluxes are determined by spatially averaging the instantaneous values on a 1º×1º grid, temporally interpolating between observed values at 1-h increments for each hour of every month, and then averaging all hour boxes in a month (Young et al., 1998; Doelling et al., 2011). Level-3 processing is performed on a nested grid, which uses 1° equal-angle regions between 45°N and 45°S, and maintains area consistency at higher latitudes. The fluxes are then output to a complete 360x180 1°×1° grid created by replication.

Table 2-1. CERES processing level descriptions.

Level	Description
0	Raw digitized instrument data for all engineering and science data streams in Consultative Committee for Space Data Systems (CCSDS) packet format.
1B	Instantaneous filtered broadband radiances at the CERES footprint resolution, geolocation and viewing geometry, solar geometry, satellite position and velocity, and all raw engineering and instrument status data.
2	Instantaneous geophysical variables at the CERES footprint resolution. Includes some Level 1B parameters and retrieved or computed geophysical variables. (e.g., filtered and unfiltered radiances, viewing geometry, radiative fluxes, imager cloud and aerosol properties).
3	Radiative fluxes and cloud properties spatially averaged onto a uniform grid. Includes either instantaneous averages sorted by local/GMT hour (e.g., SSF1deg–Hour) or temporally interpolated averages at 3–hourly, daily, monthly or monthly hourly intervals (e.g., SSF1deg–Month).
4	Level 3 data products adjusted within their range of uncertainty to satisfy known constraints (e.g., consistency between average global net TOA flux imbalance and ocean heat storage).

The CERES_EBAF_Ed2.6r product differs from previous versions of EBAF (EBAF Edition1A, Ed2.5) in that it is based upon two data products differentiated by the interpolation methods used:

(i) SSF1deg: The LW fluxes in each hour box between CERES observations are determined by linear interpolation of LW fluxes over ocean, while daytime and nighttime observations over land and desert are interpolated by fitting a half-sine curve to the observations to account for the much stronger diurnal cycle over land and desert (Young et al. 1998). The SW radiative fluxes between CERES observation times are determined from the observed fluxes by using scene-dependent diurnal albedo models, which describe how TOA albedo (and therefore flux) changes with solar zenith angle for each local time, assuming the scene properties remain invariant throughout the day. The sun angle–dependent diurnal albedo models are based upon the CERES ADMs developed for the Tropical Rainfall Measuring Mission (TRMM) satellite (Loeb et al. 2003).

(ii) SYN1deg: SW radiative fluxes between CERES observation times are determined by supplementing the CERES observations with 3-hourly TOA fluxes derived from 5 geostationary satellites. Doelling et al. (2011) provides a detailed description of how broadband TOA fluxes are derived from geostationary data.

SSF1deg provides global coverage daily with excellent calibration stability, but samples only at specific times of the day due to the sun-synchronous orbit. While the SYN1deg approach provides improved diurnal coverage by merging CERES and 3-hourly geostationary data, artifacts in the GEO data over certain regions and time periods can introduce larger uncertainties. In order to remove most of the GEO derived flux biases, the fluxes are normalized at Terra or Aqua observation times to remain consistent with the CERES instrument calibration (Doelling et al., 2011). Nevertheless, spurious jumps in the SW TOA flux record can still occur when GEO satellites are replaced due to changes in satellite position, calibration and/or visible sensor spectral response, and imaging schedules. Such artifacts in the GEO data can be problematic in studies of TOA radiation interannual variability and/or trends.

To maintain the excellent CERES instrument calibration stability of SSF1deg and also preserve diurnal information in SYN1deg, EBAF Ed2.6r uses a new approach involving scene dependent diurnal corrections to convert daily regional mean SSF1deg fluxes to diurnally complete values analogous to SYN1deg, but without geostationary artifacts. The diurnal corrections are ratios of SYN1deg-to-SSF1deg fluxes defined for each of the five geostationary satellite domains for each calendar month. They depend upon surface type and MODIS cloud fraction and height retrievals, and thus can vary from one day to the next along with the cloud properties (i.e., they are dynamic). For March 2000-June 2002, TOA fluxes are based upon CERES observations from the Terra spacecraft, while for July 2002 onwards, CERES SW observations from both Terra and Aqua are utilized in order to improve the accuracy of the diurnal corrections. In EBAF Ed1.0 and EBAF Ed2.5, only Terra data were used and the main input was either CERES SRBAVG GEO

Edition2D or CERES SYN Ed2.5, which both explicitly rely on GEO for time interpolation.

All-sky LW TOA fluxes in EBAF Ed2.6r are derived from the Terra CERES_SYN1deg-lite_Ed2.6 data product. In SYN1deg, LW radiative fluxes between CERES observation times are determined by supplementing the CERES observations with data from 5 geostationary satellites that sample every 3 hours for all longitudes between 60°S and 60°N, thus providing the most temporally and spatially complete CERES dataset for Terra or Aqua. Doelling et al. (2011) provides a detailed description of how broadband TOA fluxes are derived from geostationary data and combined with CERES observations.

The approach used to determine clear-sky TOA flux is described in detail in Loeb et al. (2009). We determine gridbox mean clear-sky fluxes using an area-weighted average of: (i) CERES/Terra broadband fluxes from completely cloud-free CERES footprints (20-km equivalent diameter at nadir), and (ii) MODIS/Terra-derived ‘‘broadband’’ clear-sky fluxes estimated from the cloud-free portions of partly and mostly cloudy CERES footprints. In both cases, clear regions are identified using the CERES cloud algorithm applied to MODIS 1-km pixel data (Minnis et al. 2011). Clear-sky fluxes in partly and mostly cloudy CERES footprints are derived using MODIS-CERES narrow-to-broadband regressions to convert MODIS narrowband radiances averaged over the clear portions of a footprint to broadband radiances. In the SW, narrow-to-broadband regressions are derived for each month. In the LW, the narrow-to-broadband regressions are developed for each calendar month from all available years of CERES data. In both SW and LW, a correction to narrow-to-broadband bias errors is made monthly based upon the difference between broadband radiances for cloud-free CERES footprints and the MODIS-based broadband estimate. This ensures that the final product’s calibration is tied to CERES. The "broadband" MODIS radiances are then converted to TOA radiative fluxes using CERES clear-sky ADMs (Loeb et al. 2005).

Despite recent improvements in satellite instrument calibration and the algorithms used to determine CERES TOA radiative fluxes, a sizeable imbalance persists in the average global net radiation at the TOA from CERES satellite observations. As in previous versions of EBAF (Loeb et al., 2009), the CERES SW and LW fluxes in EBAF Ed2.6r are adjusted within their range of uncertainty to remove the inconsistency between average global net TOA flux and heat storage in the earth–atmosphere system, as determined primarily from ocean heat content anomaly (OHCA) data. In the current version, the global annual mean values are adjusted such that the July 2005–June 2010 mean net TOA flux is 0.58±0.38 Wm^{-2} (uncertainties at the 90% confidence level) (Loeb et al., 2011a). The uptake of heat by the Earth for this period is estimated from the sum of: (i) 0.47±0.38 Wm^{-2} from the slope of weighted linear least square fit to ARGO OHCA data (Roemmich et al., 2009) to a depth of 1800 m analyzed following Lyman and Johnson (2008); (ii) 0.07±0.05 Wm^{-2} from ocean heat storage at depths below 2000 m using data from 1981–2010 (Purkey and Johnson, 2010), and (iii) 0.04±0.02 Wm^{-2} from ice warming and melt, and atmospheric and lithospheric warming (Hansen et al., 2005; Trenberth, 2009).

3.0 Cautions and Helpful Hints

The CERES Science Team notes several CAUTIONS and HELPFUL HINTS regarding the use of CERES_EBAF_Ed2.6r:

- The CERES_ EBAF_Ed2.6r product can be visualized, subsetted, and ordered from: (http://ceres.larc.nasa.gov).
- The CERES team has significantly reduced the impact of geostationary instrument artifacts in CERES_EBAF_Ed2.6r compared to earlier versions (see Section 4.0). However, users are cautioned that in the SW, CERES Terra observations are used for the period from March 2000-June 2002, while both CERES Terra and Aqua are used from July 2002 onwards. Consequently, uncertainties are slightly larger prior to July 2002.
- The solar incoming TOA flux is derived from daily SORCE TIM measurements see Section 4.7), which has an average annual flux of ~1361 Wm^{-2}, varies with time, and takes into account the solar sunspot cycle with an amplitude of ~0.1%.
- Clear-sky TOA fluxes in EBAF Ed2.6r are provided for all MODIS pixels identified as clear at 1-km spatial resolution. This definition differs from what is used in the standard CERES data products (SSF1deg and SYN1deg), which only provide clear-sky fluxes in regions that are cloud-free at the CERES footprint scale. High resolution LW TOA fluxes for clear-sky regions identified at the higher spatial resolution are on average 2.4 Wm^{-2} lower overall compared to the coarser resolution footprint case, and the regional RMS difference is 4 Wm^{-2}. SW TOA fluxes for clear-sky regions identified at the higher spatial resolution are on average 1.6 Wm^{-2} higher overall compared to the coarser resolution footprint case, and the monthly mean regional RMS difference is 6 Wm^{-2}. *Users should be aware that both of these definitions of "clear-sky" might differ from what is used in climate model output. Many models compute clear-sky radiative fluxes in each column, regardless of whether the column is clear or cloudy. Sohn et al. (2006) note that differences in how clear-sky is defined in model output and observations can lead to regional LW TOA flux differences of up to 12 W* m^{-2}.
- Clear-sky monthly mean SW and LW TOA fluxes are determined by inferring TOA fluxes at each hour of the month and averaging. SW clear-sky TOA fluxes between observation times are determined from the observed fluxes by using scene-dependent diurnal albedo models to estimate how TOA albedo (and therefore flux) changes with solar zenith angle for each local time, assuming the scene properties remain invariant throughout the day. LW clear-sky TOA fluxes between observation times are determined by linear interpolation of LW fluxes over ocean, and by applying a half-sine fit during daytime and nighttime. Therefore, monthly mean clear-sky TOA fluxes we do not explicitly account for changes in the physical properties of the scene (e.g., aerosols, surface properties) during the course of the day.

- Since TOA flux represents a flow of radiant energy per unit area, and varies with distance from the earth according to the inverse-square law, a reference level is also needed to define satellite-based TOA fluxes. From theoretical radiative transfer calculations using a model that accounts for spherical geometry, the optimal reference level for defining TOA fluxes in radiation budget studies for the earth is estimated to be approximately 20 km. At this reference level, there is no need to explicitly account for horizontal transmission of solar radiation through the atmosphere in the earth radiation budget calculation. In this context, therefore, the 20-km reference level corresponds to the effective radiative ‘‘top of atmosphere’’ for the planet. Since climate models generally use a plane-parallel model approximation to estimate TOA fluxes and the earth radiation budget, they implicitly assume zero horizontal transmission of solar radiation in the radiation budget equation, and do not need to specify a flux reference level. By defining satellite-based TOA flux estimates at a 20-km flux reference level, comparisons with plane-parallel climate model calculations are simplified since there is no need to explicitly correct plane-parallel climate model fluxes for horizontal transmission of solar radiation through a finite earth. For a more detailed discussion of reference level, please see Loeb et al. (2002).

- When the solar zenith angle is greater than 90°, twilight flux (Kato and Loeb, 2003) is added to the outgoing SW flux in order to take into account the atmospheric refraction of light. The magnitude of this correction varies with latitude and season, and is determined independently for all-sky and clear-sky conditions. In general, the regional correction is less than 0.5 W m^{-2} and the global mean correction is 0.2 W m^{-2}. Due to the contribution of twilight, there are regions near the terminator in which outgoing SW TOA flux can exceed the incoming solar radiation. Users should be aware that in these cases, albedos (derived from the ratio of outgoing SW to incoming solar radiation) exceed unity.

- EBAF uses geodetically weighting to compute global means. This spherical Earth assumption gives the well-known So/4 expression for mean solar irradiance, where S_o is the instantaneous solar irradiance at the TOA. When a more careful calculation is made by assuming the Earth is an oblate spheroid instead of a sphere, and the annual cycle in the Earth's declination angle and the Earth-sun distance are taken into account, the division factor becomes 4.0034 instead of 4.

- The following file provides the zonal geodetic weights used to determine global mean quantities.
(http://ceres.larc.nasa.gov/science_information.php?page=GeodeticWeights).

- EBAF clear-sky LW TOA fluxes exhibit a sharp decline of approximately 0.25 Wm^{-2} relative to CERES SYN1deg-lite in 2008 (see Figure 5-2). We believe this is due to sensitivity of the CERES nighttime cloud mask (which uses MODIS pixel data) to a change in meteorological assimilation data from GEOS-4 to GEOS-5 starting in January 2008. A consistent GEOS-5 assimilation system will be used throughout the CERES record in the Edition4 release, which is scheduled for data processing in early 2012.

4.0 Accuracy and Validation

4.1 Global Mean TOA Flux Comparisons

Table 4-1 compares global TOA averages for EBAF Ed2.6r with earlier versions EBAF Ed1.0, EBAF Ed2.5 and EBAF Ed2.6. All-sky SW TOA flux in Ed2.6r is 0.5 Wm^{-2} greater than Ed1.0 and 0.3–0.4 Wm^{-2} greater than Ed2.5. The main difference between all-sky SW TOA fluxes in EBAF Ed2.6r and Ed2.5 is that Ed2.6r uses the methodology described in Section 5.1, while EBAF Ed2.5 is derived from SYN1deg-lite Ed2.5, which relies explicitly on geostationary satellite measurements to complete the diurnal cycle. Another difference that applies to all TOA flux variables is that EBAF Ed2.6r applies geodetic weighting when averaging globally, while geocentric weighting is assumed in EBAF Ed2.5 and EBAF Ed1.0.

Clear-sky LW TOA flux in Ed2.6r is 0.3 Wm^{-2} greater than Ed2.5 and 2.6r Wm^{-2} smaller than Ed1.0. The difference between EBAF Ed2.6r and Ed2.5 is due to geodetic versus geocentric weighting discussed above. In EBAF Ed1.0, geocentric weighting is assumed and the methodology for time-space averaging differs from that in Ed2.5 and Ed 2.6r. In EBAF Edtion2.5A, monthly mean high-resolution clear-sky SW and LW TOA fluxes are determined using a different time-space averaging technique compared to EBAF Edition1A. Each day, instantaneous clear-sky TOA fluxes are sorted by local time and averaged over an equal-area 1°×1° latitude-longitude grid. A modified version of the production code used to produce CERES SRBAVG and SSF1deg-lite_Ed2.5 clear-sky fluxes is now used to determine monthly mean high-resolution clear-sky SW and LW TOA fluxes in EBAF Edtion2.5A. In EBAF Edition1A, the monthly mean clear-sky TOA fluxes were inferred from daily means without sorting by local time first, resulting in larger uncertainties at mid-to-high latitudes where multiple overpasses per day occur at different local times.

Table 4-1. Global mean TOA fluxes from EBAF Ed1.0, EBAF Ed2.5, EBAF Ed2.6 and EBAF 2.6r for March 2000-February 2005 and March 2000-February 2010.

	March 2000–February 2005			
	EBAF Ed1.0	**EBAF Ed2.5**	**EBAF Ed2.6**	**EBAF Ed2.6r**
Incoming Solar	340.0	340.2	340.5	340.0
LW (all-sky)	239.6	239.6	239.9	239.7
SW (all-sky)	99.5	99.7	100.0	99.8
Net (all-sky)	0.85	0.85	0.55	0.54
LW (clear-sky)	269.1	266.2	266.5	266
SW (clear-sky)	52.9	52.4	52.6	52.5
Net (clear-sky)	18.0	21.5	21.4	21.5
	March 2000–February 2010			
	EBAF Ed1.0	**EBAF Ed2.5**	**EBAF Ed2.6**	**EBAF Ed2.6r**
Incoming Solar		340.1	340.4	339.9
LW (all-sky)		239.6	239.9	239.6
SW (all-sky)		99.5	99.9	99.7
Net (all-sky)		1.0	0.59	0.57
LW (clear-sky)		266.0	266.4	265.9
SW (clear-sky)		52.4	52.5	52.5
Net (clear-sky)		21.6	21.5	21.5

4.2 Regional Mean All-Sky SW TOA Flux

Figures 4-1 (a) and (b) provide regional plots of mean SW TOA flux and interannual variability for the month of March based upon all March months between 2000 and 2010. The regional 1°x1° standard deviation ranges from near zero at the poles to 40 Wm^{-2} in the western tropical Pacific Ocean region. Considering all 1°x1° regions, the overall global regional standard deviation in SW TOA flux is 22 Wm^{-2}, and the overall global mean SW TOA flux is 99.7 Wm^{-2}.

The uncertainty in 1°x1° regional SW TOA flux is evaluated separately for 03/2000-06/2002 (Terra-Only period) and for 07/2002-12/2010 (Terra-Aqua period). To determine uncertainties for the Terra-Only period, we use data from the Terra-Aqua period and compare regional fluxes derived by applying diurnal corrections to the Terra SSF1deg product with regional fluxes determined by averaging fluxes from the Terra and Aqua SYN1deg Ed2.6 data products. The SYN1deg Ed2.6 products combine CERES observations on Terra or Aqua with five geostationary instruments covering all longitudes between 60°S and 60°N, thus providing the most temporally and spatially complete CERES dataset for Terra or Aqua. Figures 4-2 (a) and (b) show maps of the regional bias and RMS error. The overall regional RMS error is 4 Wm^{-2}. In stratocumulus regions, RMS differences are typically around 5 Wm^{-2}, or approximately 5% of the regional mean value.

Uncertainties for the Terra-Aqua period are determined by comparing regional fluxes derived by applying diurnal corrections to the average of Terra and Aqua SSF1deg Ed2.6 fluxes with average Terra and Aqua regional fluxes from SYN1deg Ed2.6. Results, in Figures 4-3 (a) and (b), show much improvement over the Terra-only case in Figure 4-2, with regional errors decreasing to 2.7 Wm^{-2} overall, and errors < 3 Wm^{-2} in stratocumulus regions.

To place the above results into context, regional mean and RMS differences between Terra and Aqua SYN1deg Ed2.6 SW TOA fluxes are provided in Figures 4-4 (a) and (b). Overall, the RMS difference is 4.4 Wm^{-2}. RMS differences >10 Wm^{-2} are evident over Africa, Tibet and over isolated regions in the Americas. Since the same geostationary data are used for both Terra and Aqua SYN1deg products, why should there be any discrepancy? The regional discrepancies are mainly associated with the regional normalization of 3-hourly geostationary data to either Terra or Aqua anchor measurements can have a time mismatch of up to 1.5 hours, causing cloud conditions and fluxes to differ (Doelling et al., 2011). Consequently, a longitudinal striping pattern appears that is correlated with the time separation between the geostationary and sun-synchronous observations.

If we assume the overall uncertainty is due to the EBAF diurnal correction, the combined sum of the Terra and Aqua SYN1deg Ed2.6 SW regional fluxes, which is given by the RMS difference between Terra and Aqua SYN1deg divided by the square root of 2, and CERES instrument calibration uncertainty of 1 Wm^{-2} (1σ), the regional uncertainty for EBAF Ed2.6 for March 2000–June 2002 is $\text{sqrt}(4^2+(4.4/2)^2+1^2)$ or approximately 5 Wm^{-2}, and for July 2002-December 2010 is $\text{sqrt}(2.7^2+(4.4/2)^2+1^2)$ or 4 Wm^{-2}.

While the diurnal corrections applied to SSF1deg Ed2.6 fluxes do introduce a slight increase regional SW TOA flux uncertainty, they dramatically improve the EBAF record by minimizing the impact of geostationary satellite artifacts, especially with respect to temporal regional trends. As an example, Figures 4-5 (a) and (b) show regional trends in SW TOA flux for from EBAF Ed2.6 and SYN Ed2.6 for March 2000–December 2010. In Figure 4-5 (b), vertical lines corresponding to geostationary satellite boundaries are clearly visible around 30°E, 100°E, 180°E, 105°W and 40°W. The geostationary artifacts

are more pronounced over Africa and Asia, but also show up to the east of South America. In contrast, the geostationary artifacts are largely absent in Figure 4-5 (a), which is based upon EBAF Ed2.6 data. Figures 4-6 (a) and (b) provide SW TOA flux anomaly differences between SYN1deg and SSF1deg Ed2.6 as well as EBAF and SSF1deg Ed2.6 for 60°S-60°N (Figure 4-6 (a)) and the same latitude range but restricted to 101.5°E–140°E (Figure 4-6 (b)). The latter region covers much of the Western Tropical Pacific Ocean region, Indonesia, and East Asia. In both cases, the SYN1deg Ed2.6 results show a sharp decline relative to SSF1deg Ed2.6 reaching 0.4 Wm^{-2} per decade for 60°S-60°N and 1.8 Wm^{-2} per decade in the smaller region. In both cases, the new EBAF2.6 results remain well within 0.1 Wm^{-2} per decade of SSF1deg Ed2.6, while accounting for the diurnal cycle.

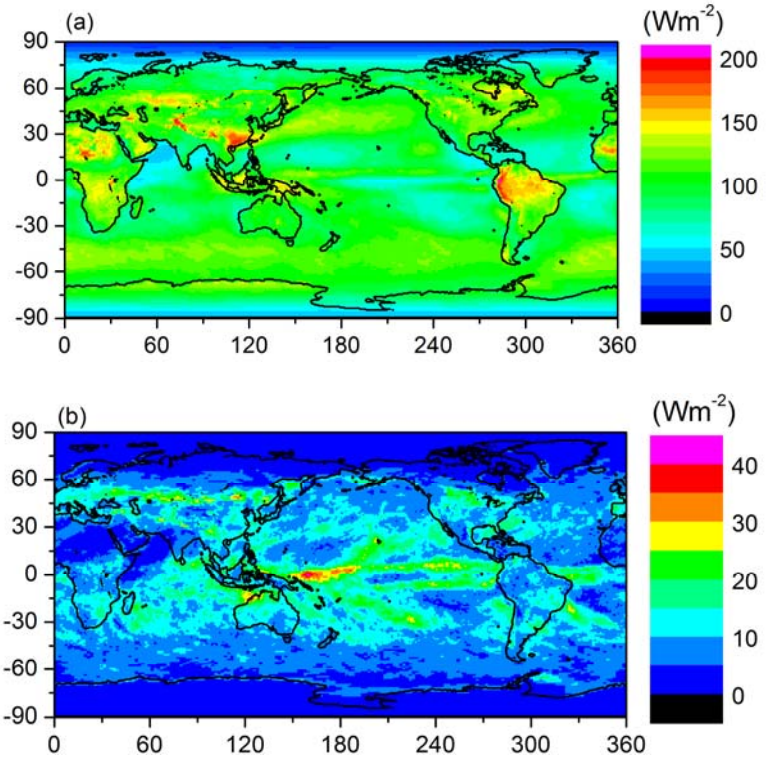

Figure 4-1. (a) Average and (b) standard deviation of SW TOA flux determined from all March months from 2000-2010 using the CERES EBAF2.6 product.

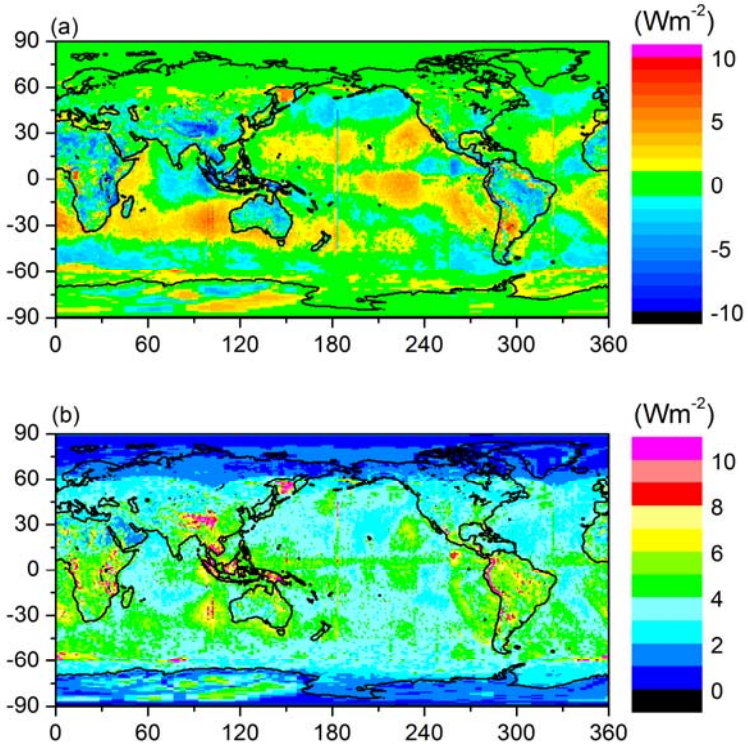

Figure 4-2. (a) Bias and (b) RMS difference between fluxes derived by applying diurnal corrections to Terra SSF1deg Ed2.6 and TOA fluxes from the average of Terra and Aqua SYN1 deg.

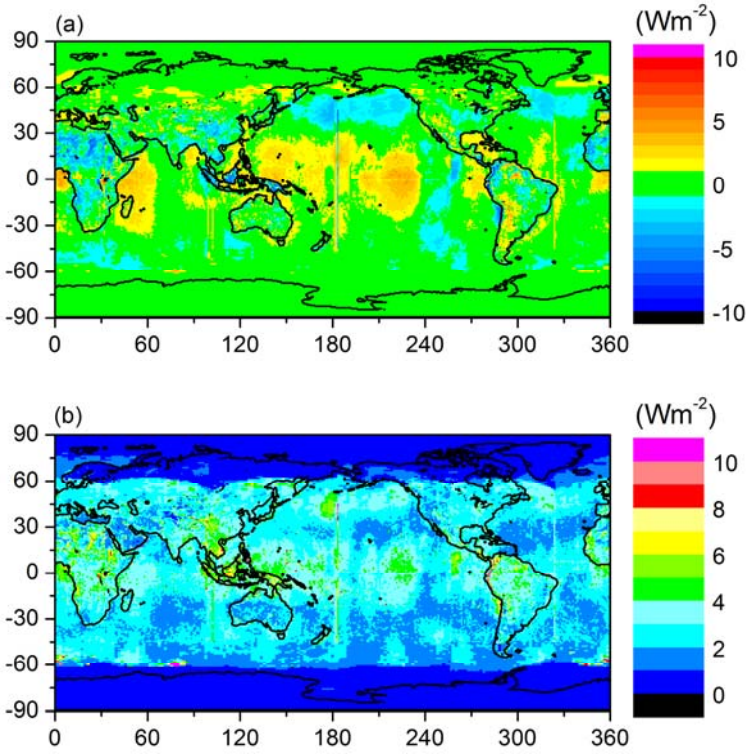

Figure 4-3. Same as Figure 4-2 but after applying diurnal corrections to combined Terra+Aqua SSF1deg Ed2.6 fluxes.

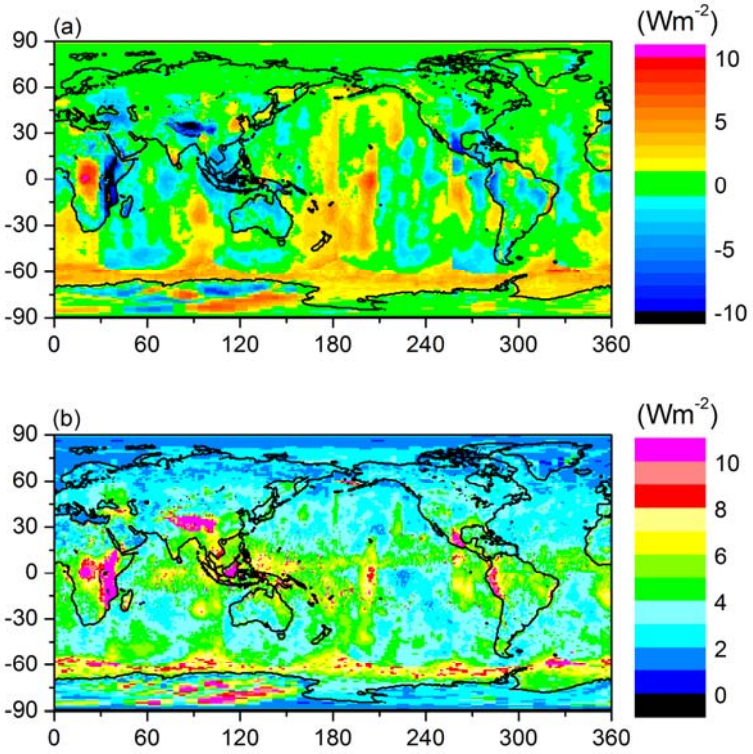

Figure 4-4. (a) Mean and (b) RMS difference between SW TOA fluxes from CERES Terra and CERES Aqua SYN1deg Ed2.6 data products.

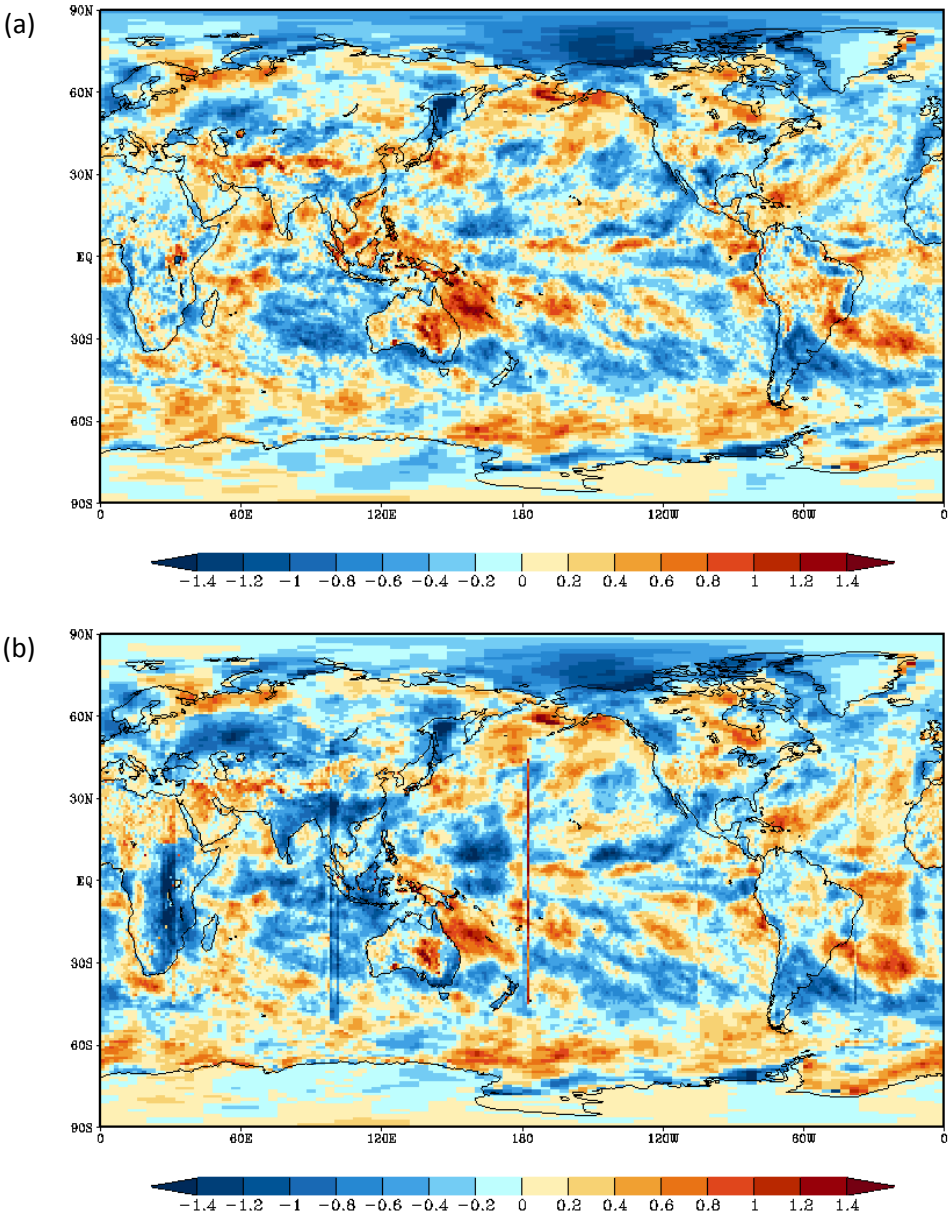

Figure 4-5. Regional trends (Wm^{-2} per year) in SW TOA flux for March 2000-December 2010 from (a) EBAF Ed2.6 and (b) SYN1deg Ed2.6.

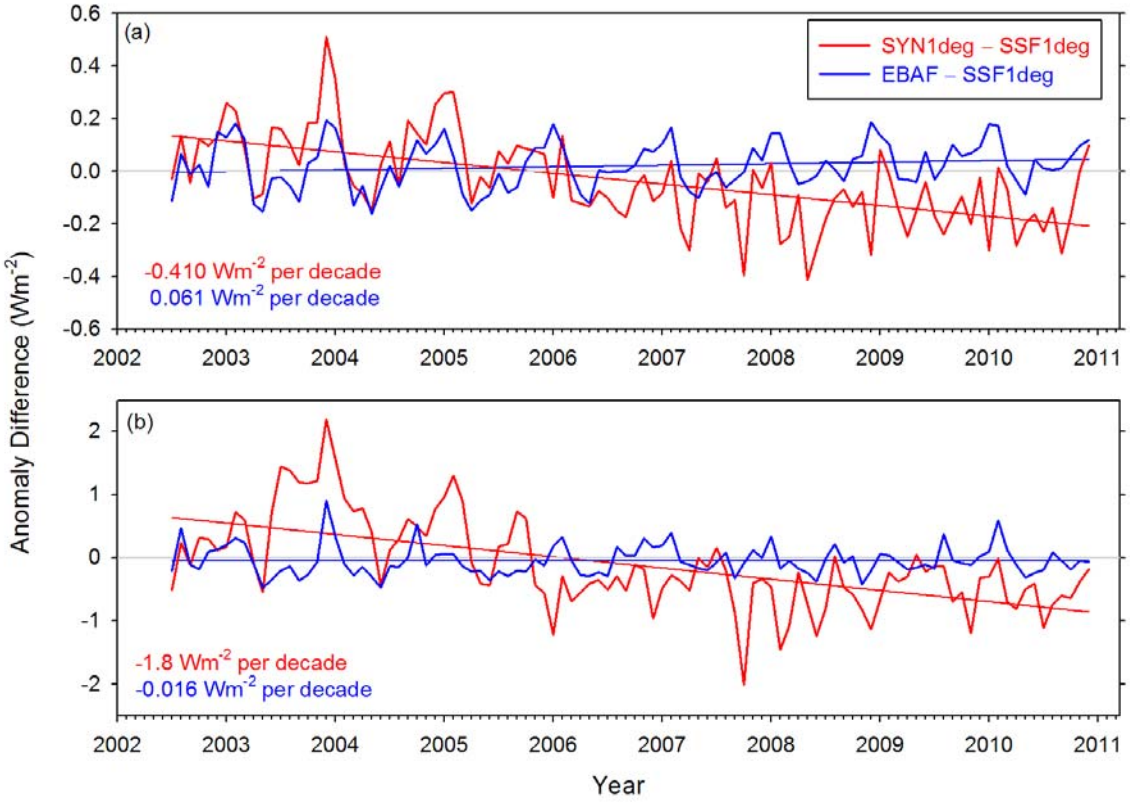

Figure 4-6. SW TOA flux anomaly difference between SYN1deg and SSF1deg Ed2.6 and between EBAF and SSF1deg Ed2.6 for (a) 60°S-60°N, and (b) the western sector of the region covered by GMS-5, GOES-9, and MTSAT-1R geostationary satellites (60°S-60°N, 101.5°E-140°E) for July 2002-December 2010. Straight lines correspond to least square fits through the anomaly difference curves. Slopes are in units Wm^{-2} per decade.

4.3 Regional Mean All-Sky LW TOA Flux

Figures 4-7 (a) and (b) provide regional plots of mean LW TOA flux and interannual variability for the month of March based upon all March months between 2000 and 2010. The regional standard deviation ranges from near zero at the poles to 30 Wm^{-2} in the equatorial Pacific Ocean region. Considering all 1°x1° regions between 90°S×90°N, the overall regional standard deviation in LW TOA flux is 17 Wm^{-2}, and the overall global mean LW TOA flux is 238 Wm^{-2}.

The uncertainty in 1°x1° regional LW TOA flux is evaluated using data from 07/2002-12/2010, when CERES instruments on both Terra and Aqua were operating. We compare regional fluxes from Terra and Aqua SYN1deg Ed2B products directly in Figures 4-8 (a) and (b). The overall mean difference is 0.05 Wm^{-2} and regional RMS difference is 2 Wm^{-2}. Regional differences can reach 5 Wm^{-2} in isolated regions of convection over south and central Africa and in the west Pacific Ocean region (Figure 4-8 (b)).

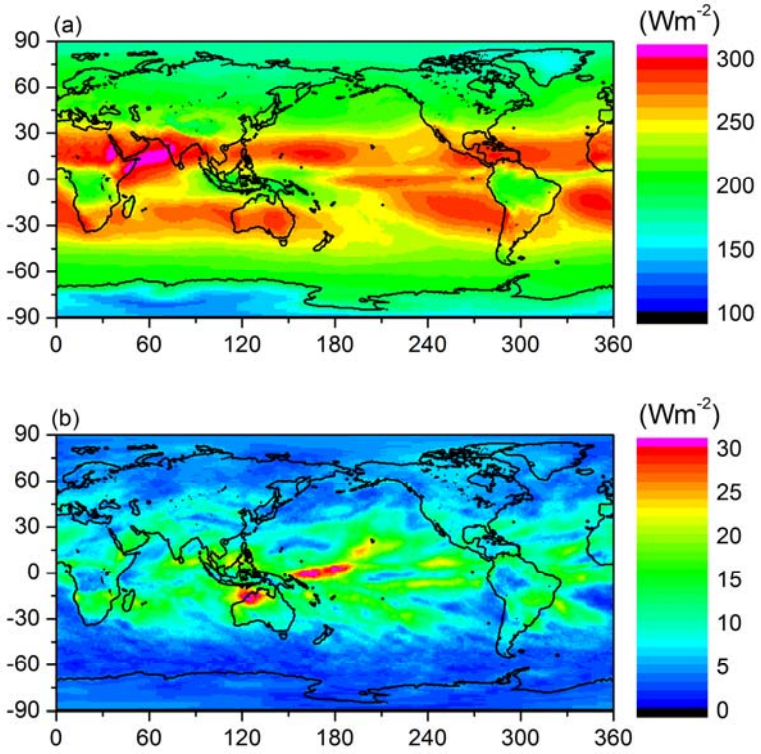

Figure 4-7. (a) Average and (b) standard deviation of LW TOA flux determined from all March months from 2000-2010 using the CERES EBAF2.6 product.

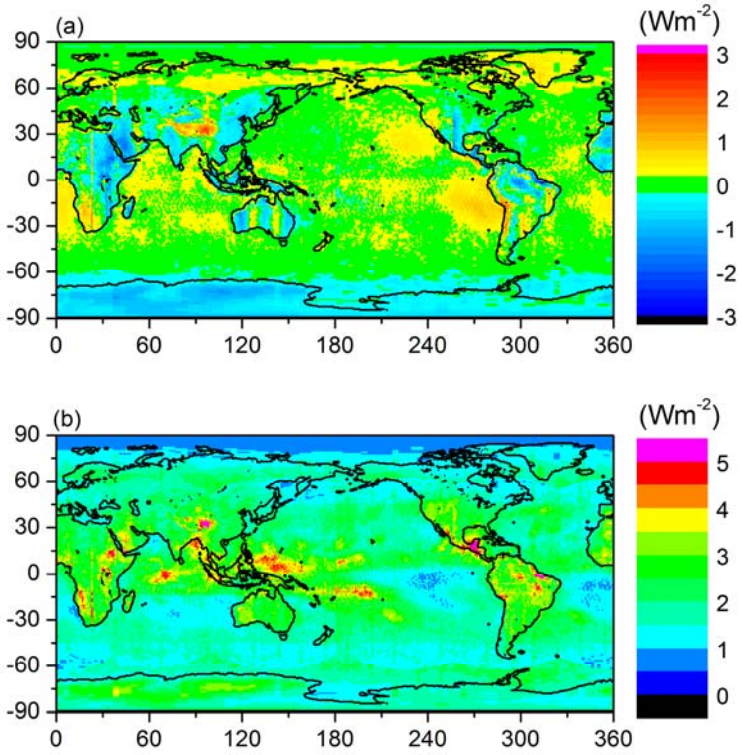

Figure 4-8. (a) Bias and (b) RMS difference between LW TOA fluxes from Terra and Aqua SYN1 deg Ed2.6 data products.

4.4 Regional Mean Clear-Sky SW

Figures 4-9 (a) and (b) provide regional plots of mean clear-sky SW TOA flux and interannual variability for the month of March based upon all March months between 2000 and 2010. The regional 1°x1° standard deviation ranges from near zero over remote ocean regions to 35 Wm^{-2} over mid-latitude land regions, associated with seasonal snow. Considering all 1°x1° regions, the overall global regional standard deviation in SW clear-sky TOA flux is 22 Wm^{-2}, and the overall global mean is 54 Wm^{-2}.

The uncertainty in 1°x1° regional SW clear-sky TOA flux is determined from calibration uncertainty, error in narrow-to-broadband conversion, ADM error, time-space averaging, and scene identification. For CERES, calibration uncertainty is 1% (1σ), which for a typical global mean clear-sky SW flux corresponds to ≈0.5 Wm^{-2}. Figures 4-10 (a) and (b) show the regional distribution of the correction used to correct for regional narrow-to-broadband error. This is derived by applying narrow-to-broadband regressions to MODIS visible radiances for completely cloud-free CERES footprints and then comparing the estimated broadband flux with CERES. The overall bias is 0.2 Wm^{-2} and the regional RMS difference is 0.65 Wm^{-2}. Assuming a 50% error in the correction, the narrowband-to-broadband contribution to regional uncertainty becomes 0.3 Wm^{-2}. For

clear-sky SW TOA flux, ADM error contributes 1 Wm^{-2} to regional RMS error (Loeb et al., 2007), and time-space averaging adds 2 Wm^{-2} uncertainty. The latter is based upon an estimate of the error from TRMM-derived diurnal albedo models that provide albedo dependence upon scene type (Loeb et al., 2003). In EBAF, "clear-sky" is defined as cloud-free at the MODIS pixel scale (1 km). A pixel is identified as clear using spectral MODIS channel information and a cloud mask algorithm (Minnis et al., 2011). Based upon a comparison of SW TOA fluxes for CERES footprints identified as clear according to MODIS but cloudy according to CALIPSO, and TOA fluxes from footprints identified as clear according to both MODIS and CALIPSO, Sun et al. (2011) found that footprints with undetected subvisible clouds reflect 2.5 Wm^{-2} more SW radiation compared to completely cloud-free footprints, and occur in approximately 50% of footprints identified as clear by MODIS. This implies an error of 1.25 Wm^{-2} due to misclassification of clear scenes. The total error in TOA outgoing clear-sky SW radiation in a region is $\text{sqrt}(0.5^2+0.3^2+1^2+2^2+1.25^2)$ or approximately 3 Wm^{-2}.

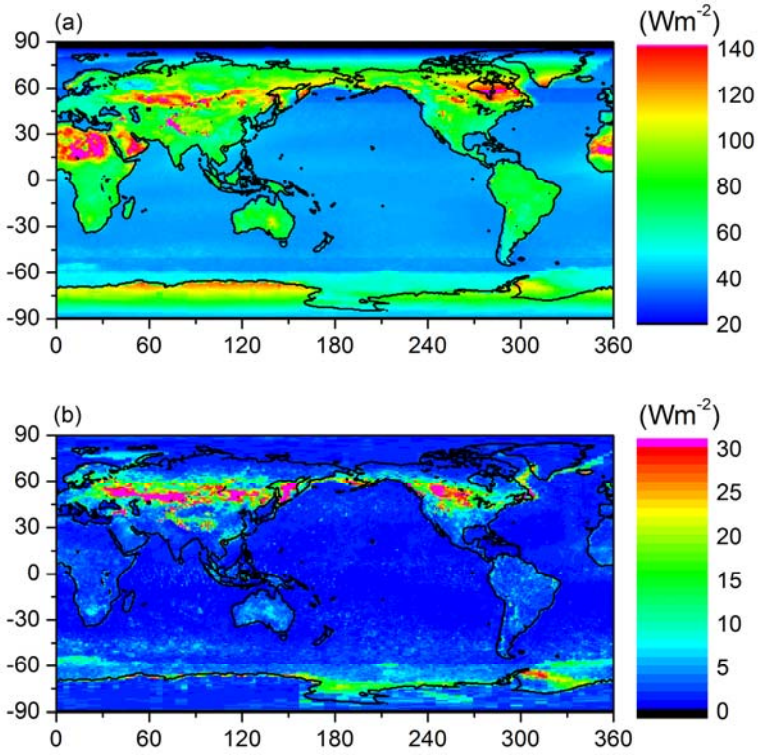

Figure 4-9. (a) Average and (b) standard deviation of SW clear-sky TOA flux determined from all March months from 2000-2010 using the CERES EBAF2.6 product.

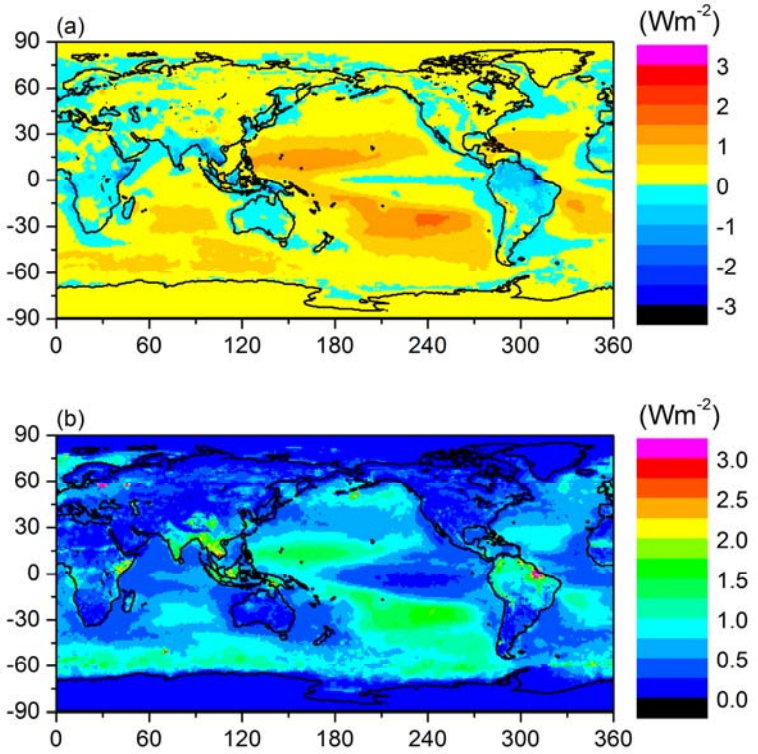

Figure 4-10. (a) Bias and (b) RMS difference between high-resolution TOA clear-sky fluxes derived with and without corrections for regional narrow-to-broadband error.

4.5 Regional Mean Clear-Sky LW

Figures 4-11 (a) and (b) provide regional plots of mean clear-sky LW TOA flux and interannual variability for the month of March based upon all March months between 2000 and 2010. The regional 1°x1° standard deviation ranges from near zero at the poles to 30 Wm^{-2} in mountainous regions. Considering all 1°x1° regions, the overall global regional standard deviation in LW TOA flux is 10 Wm^{-2}, and the overall global mean LW TOA flux is 264 Wm^{-2}.

The uncertainty in 1°x1° regional LW clear-sky TOA flux is determined from calibration uncertainty, error in narrow-to-broadband conversion, ADM error, time-space averaging, and scene identification. For CERES, calibration uncertainty is 0.5% (1σ), which for a typical global mean clear-sky LW flux corresponds to ≈1 Wm^{-2}. Figures 4-12 (a) and (b) show the regional distribution of the correction used to correct for regional narrow-to-broadband error. This is derived by applying narrow-to-broadband regressions to MODIS infrared radiances for completely cloud-free CERES footprints and then comparing the estimated broadband flux with CERES. The overall bias is -0.5 Wm^{-2} and the regional RMS difference is 2.5 Wm^{-2}. Assuming a 50% error in the correction, the narrowband-to-broadband contribution to regional uncertainty becomes 1.74 Wm^{-2}. For clear-sky LW TOA flux, ADM error contributes 0.7 Wm^{-2} to regional RMS error (Loeb et al., 2007), and time-space averaging adds 1 Wm^{-2} uncertainty. The latter assumes zero error over ocean (i.e., no diurnal appreciable diurnal cycle in clear-sky LW) and a 3 Wm^{-2}

error in the half-sine fit over land and desert (Young et al., 1998). In EBAF, "clear-sky" is defined as cloud-free at the MODIS pixel scale (1 km). A pixel is identified as clear using spectral MODIS channel information and a cloud mask algorithm (Minnis et al., 2011). Based upon a comparison of LW TOA fluxes for CERES footprints identified as clear according to MODIS but cloudy according to CALIPSO, and TOA fluxes from footprints identified as clear according to both MODIS and CALIPSO, Sun et al. (2011) found that footprints with undetected subvisible clouds emit 5.5 Wm^{-2} less LW radiation compared to completely cloud-free footprints, and occur in approximately 50% of footprints identified as clear by MODIS. This implies an error of 2.75 Wm^{-2} due to misclassification of clear scenes. The total error in TOA outgoing clear-sky LW radiation in a region is sqrt(1^2+1.74^2+0.7^2+1^2+2.75^2) or approximately 3.6 Wm^{-2}.

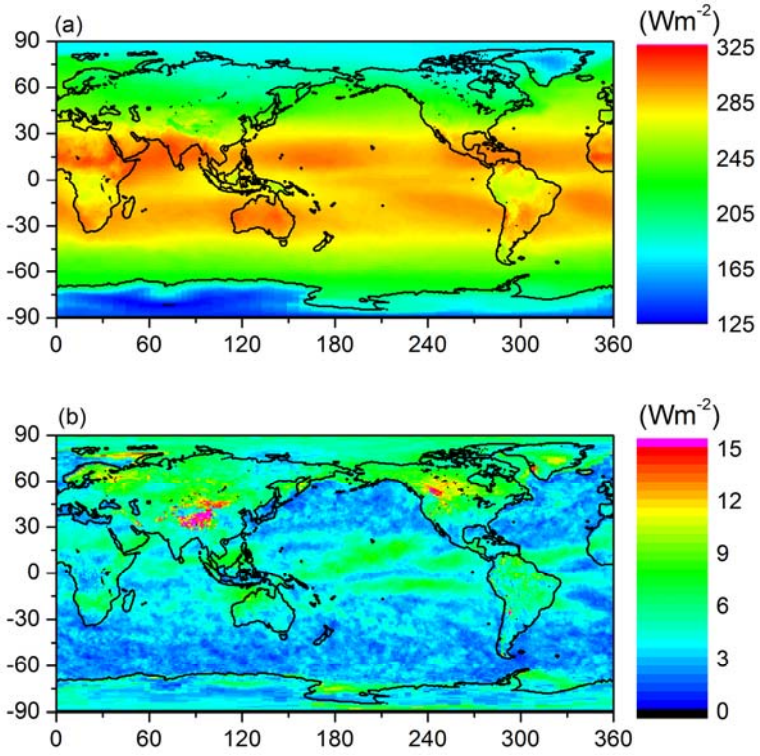

Figure 4-11. (a) Average and (b) standard deviation of LW TOA flux determined from all March months from 2000-2010 using the CERES EBAF2.6 product.

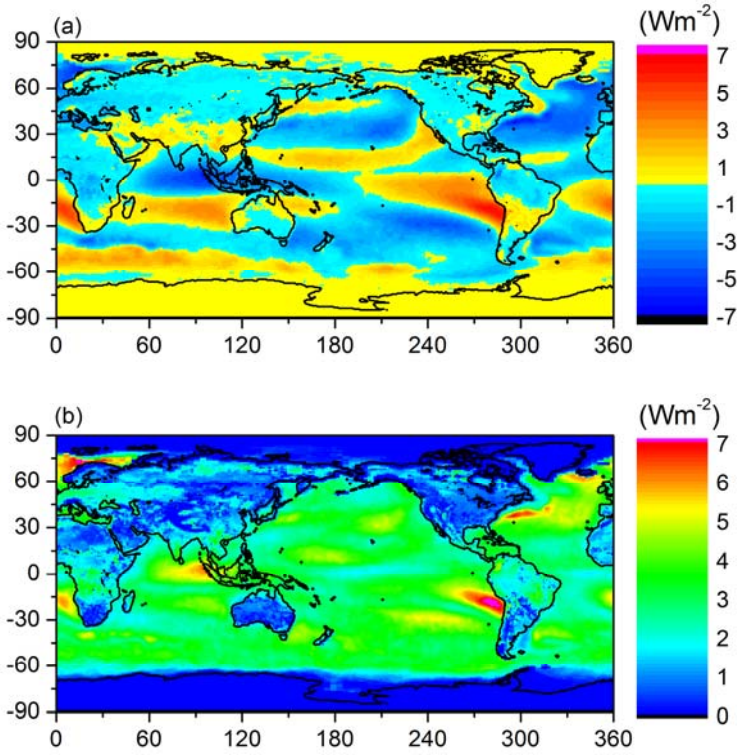

Figure 4-12. (a) Bias and (b) RMS difference between high-resolution TOA clear-sky fluxes derived with and without corrections for regional narrow-to-broadband error.

4.6 Clear-Sky TOA Flux Dependence Upon Spatial Resolution

Figure 4-13 shows how including clear-sky TOA fluxes at spatial scales smaller than a CERES footprint affects regional TOA fluxes. It shows the difference between CERES/MODIS based high-resolution clear-sky TOA prior to making any adjustments like those in Eqs. (1) and (2) and SYN1deg-lite_Ed2.5 for March 2006 (similar results are obtained with SYN1deg-lite_Ed2.6). In the SW, differences are greatest over eastern Asia and southern Africa for land and just west of the Saharan desert over ocean. Large differences are also found over the Southern Ocean where clear-sky sampling at CERES footprint scales is low. High-resolution CERES/MODIS clear-sky LW TOA fluxes are generally lower than those in SYN1deg-lite_Ed2.5, especially in regions where precipitable water is large. Note how the regional pattern of clear-sky LW TOA flux differences closely follows the regional precipitable water distribution (Figure 4-13 middle and bottom panels).

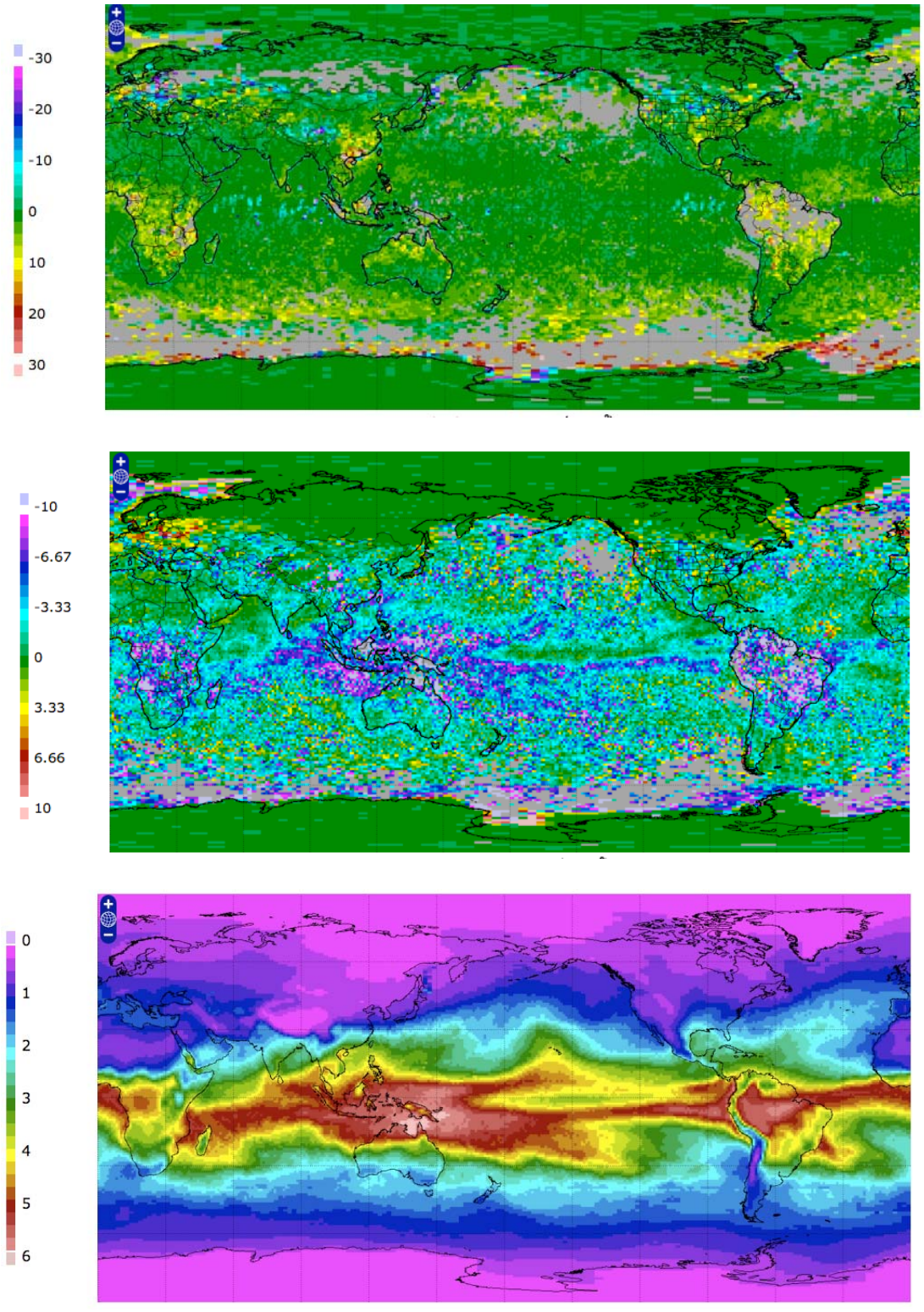

Figure 4-13. Clear-sky TOA flux difference between high resolution CERES/MODIS and SYN1deg-lite_Ed2.5 for SW (top) and LW (middle). Bottom panel shows precipitable water in mm.

4.7 Solar Incoming

The CERES science team provides monthly regional mean TOA incident shortwave radiation derived from the Total Solar Irradiance (TIM) instrument aboard the Solar Radiation and Climate Experiment (SORCE) satellite. The TIM instrument measures the absolute intensity of solar radiation, integrated over the entire solar disk and the entire solar spectrum reported at the mean solar distance of 1 astronomical unit (AU). The CERES product uses the daily fluxes from the SORCE web site at : http://lasp.colorado.edu/sorce/tsi_data/daily/sorce_tsi_L3_c24h_latest.txt from February 25, 2003 until Dec 31, 2010 using version 11. The daily fluxes are updated from this site on a regular basis and there usually is a 2-month data lag from real-time. From March 2000 until February 24, 2003 the composite_d41_62_0906.dat dataset from Froehlich and Lean 1998 is used with an offset value of -4.4388599 Wm^{-2} to put the daily fluxes on the same radiometric scale as SORCE. These are available from: ftp://ftp.pmodwrc.ch/pub/data/irradiance/composite/. The Froehlich and Lean fluxes are derived from 6 independent space based radiometers since 1978 using overlap time periods to normalize the fluxes to a common reference. The fluxes are observed from the Hickey-Frieden (HF), Active Cavity Radiometer Irradiance Monitor (ACRIM 1, II and III), Earth Radiation Budget Satellite (ERBS) and Variability of solar Irradiance and Gravity Oscillations (VIRGO) missions. The basis for 2000-2003 was mainly from VIRGO. Figure 4-14 displays the SORCE data in red and the pre-SORCE solar irradiance records adjusted to SORCE composite daily fluxes in blue.

The TIM Total Solar Irradiance (TSI) measurements monitor the incident sunlight to the Earth's atmosphere using an ambient temperature active cavity radiometer. Using electrical substitution radiometers (ESRs) and taking advantage of new materials and modern electronics, the TIM measures TSI to an estimated absolute accuracy of 350 ppm (0.035%). Relative changes in solar irradiance are measured to less than 10 ppm/yr (0.001%/yr), allowing determination of possible long-term variations in the Sun's output (Kopp et al. 2005).

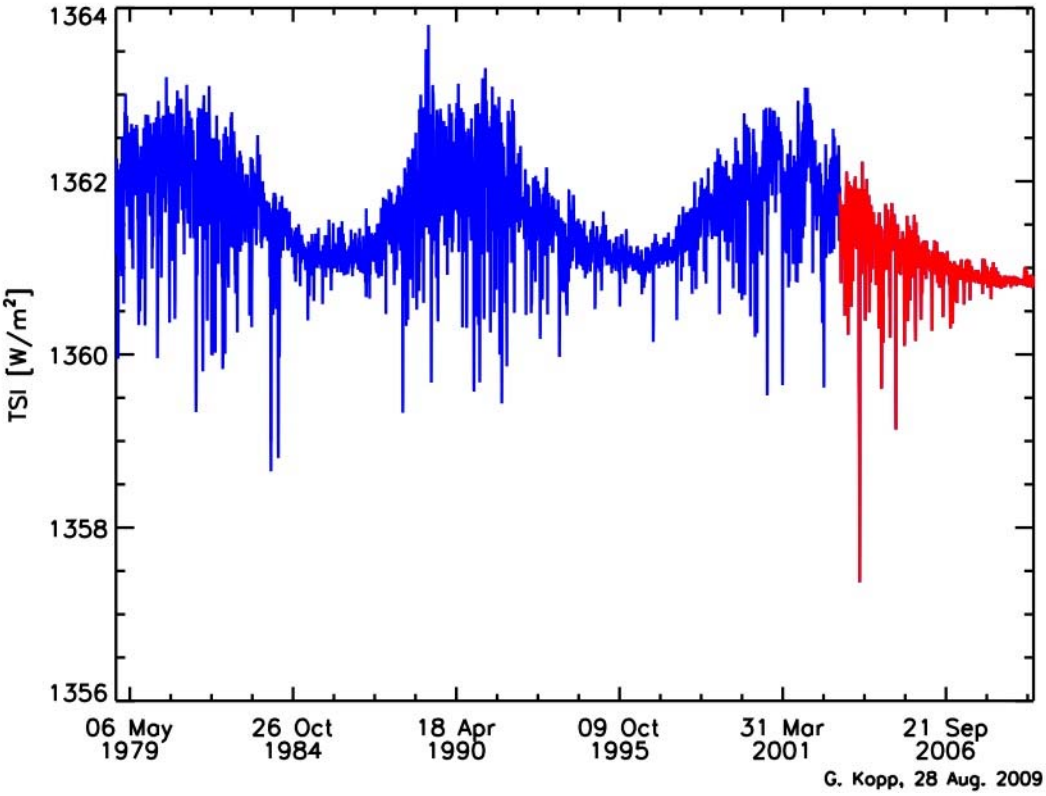

Figure 4-14. The Froehlich and Lean (1998) composite TOA solar incoming fluxes in blue and the SORCE TIM daily fluxes in red beginning on February 25, 2003.

5.0 Version History Summary

Table 5-1 provides a list of input data products used to create each version of EBAF and also lists the reference providing the global energy imbalance constraint used to anchor the CERES TOA fluxes.

Table 5-1. EBAF Input and Heating Rate Constraint.

Version	SW all-sky	LW all-sky	Clear-sky	Global Energy Imbalance Constraint
Ed 1	Terra-SYN1deg Ed2.0 (SRBAVG)	Terra-SYN1deg Ed2 (SRBAVG)	Terra-SYN1deg Ed2 (SRBAVG)	Hansen 2005
Ed 2.5	Terra-SYN1deg Ed2.5	Terra-SYN1deg Ed2.5	Terra-SSF1deg Ed2.5	Hansen 2005
Ed 2.6 & Ed2.6r	Terra/Aqua-SSF/SYN1deg Ed2.6 (see above)	Terra-SYN1deg Ed2.6	Terra-SSF1deg Ed2.6	ARGO based 2006-2010 (See above)

5.1 Difference between EBAF Ed2.6r and EBAF Ed2.6

(a) Global Mean Calculation

In EBAF Ed2.6 a code error in the global mean calculation of all variables was discovered. The root cause was the use of incorrect zonal weights in the integration of global mean quantities. The problem was corrected in EBAF Ed2.6r by using correct zonal weights for an oblate spheroid Earth (http://ceres.larc.nasa.gov/science_information.php?page=GeodeticWeights).

Figure 5-1 (a) compares the difference between global mean solar irradiance for EBAF 2.6 and EBAF Ed2.6r. Global mean differences exhibit a seasonal cycle with maximum occurring in June and minimum in December. The code error does not impact deseasonalized anomalies in global mean quantities, as illustrated in Figure 5-1 (b).

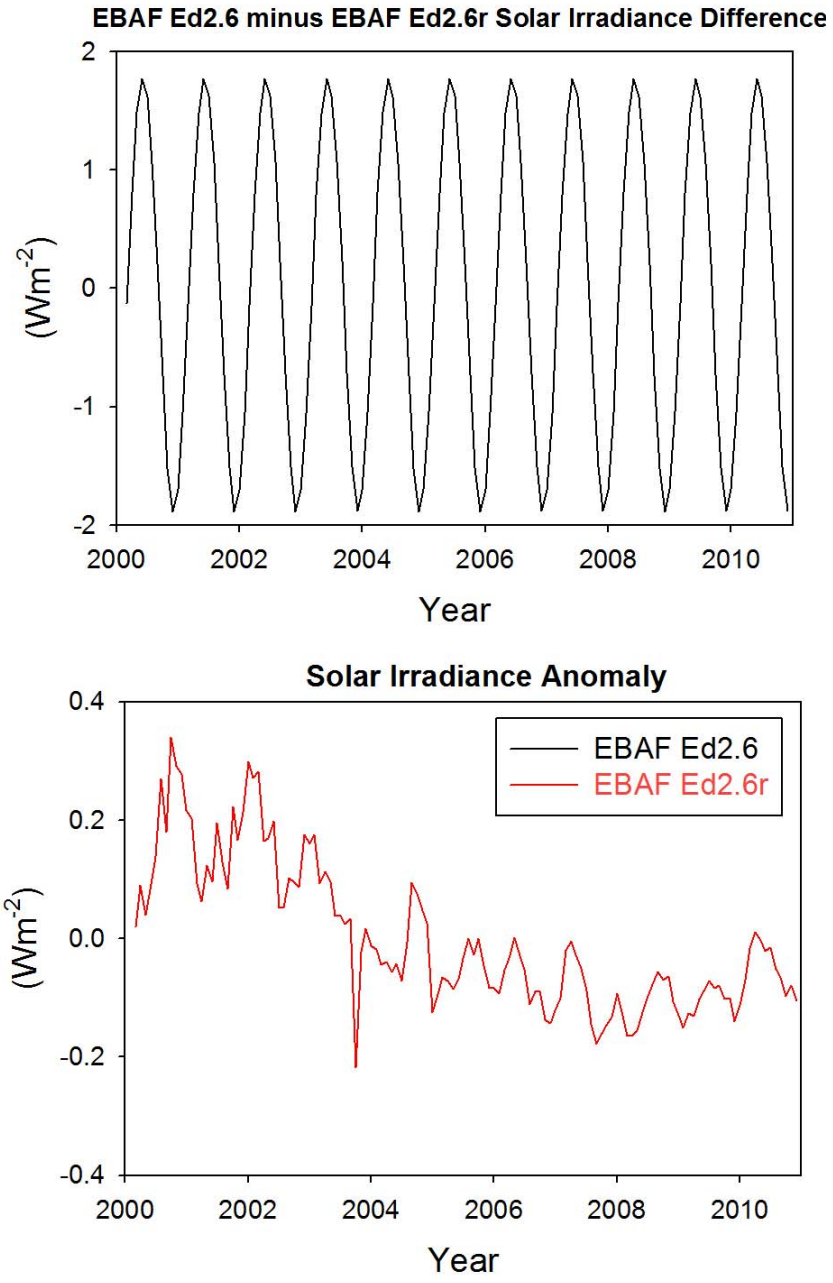

Figure 5-1. (a) EBAF Ed2.6 minus EBAF Ed2.6r global mean solar irradiance difference; (b) Anomalies in solar irradiance from EBAF Ed2.6 and EBAF Ed2.6r.

(b) Clear-sky LW TOA Fluxes

Deseasonalized anomalies in clear-sky LW TOA flux from EBAF Ed2.6 show a marked discontinuity after 2008 relative to anomalies in SSF1deg Ed2.6 (Figure 5-1 (a)). The problem is associated with greater sampling uncertainties in the monthly narrow-to-

broadband coefficients after 2008 due to a decrease in cloud cover during this period. To overcome this problem, LW narrow-to-broadband regressions are re-derived in EBAF Ed2.6r for each calendar month using all data from March 2000 through June 2011. Monthly regional bias errors are removed using difference maps of broadband and narrow-to-broadband cloud-free TOA fluxes at the CERES footprint scale. This ensures that the final product's calibration is tied to CERES. After applying this modified approach, anomalies from EBAF Ed2.6r are closer to SSF1deg-lite Ed2.6 (Figure 5-1 (b)), and show no discontinuity after 2008. Further, anomalies are less noisy compared to Ed2.6.

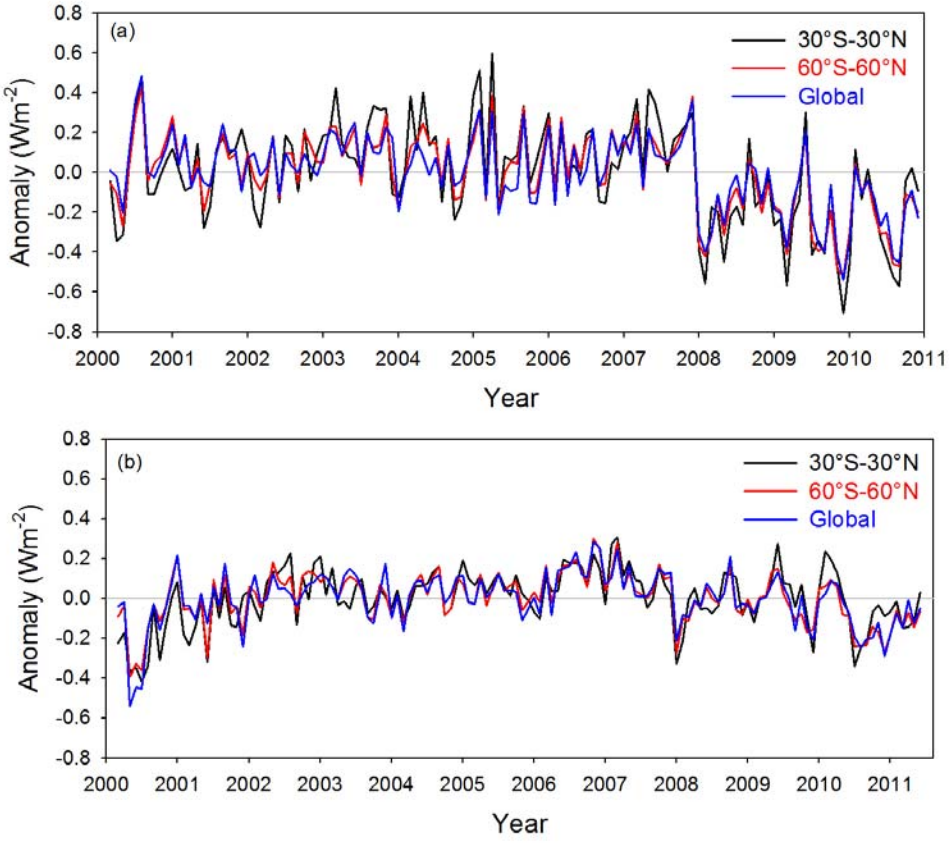

Figure 5-2. Anomaly of clear-sky LW TOA flux difference between (a) EBAF Ed2.6 and SSF1deg-lite Ed2.6 for March 2000–December 2010 and (b) EBAF Ed2.6r and SSF1deg-lite Ed2.6 for March 2000–June 2011.

5.2 Other Differences Amongst Earlier Versions of EBAF

The main impact of the Edition 2.5 calibration changes to EBAF is to improve the calibration stability of the record. Another significant difference between EBAF Edition1A and Edition2.5A is in clear-sky, particularly in the LW.

In EBAF Edtion2.5A, monthly mean high-resolution clear-sky SW and LW TOA fluxes are determined using a different time-space averaging technique compared to EBAF Edition1A. Each day, instantaneous clear-sky TOA fluxes are sorted by local time and averaged over an equal-area 1°×1° latitude-longitude grid. A modified version of the production code used to produce CERES SRBAVG and SSF1deg-lite_Ed2.5 clear-sky fluxes is now used to determine monthly mean high-resolution clear-sky SW and LW TOA fluxes in EBAF Edtion2.5A. In EBAF Edition1A, the monthly mean clear-sky TOA fluxes were inferred from daily means without sorting by local time first, resulting in larger uncertainties at mid-to-high latitudes where multiple overpasses per day occur at different local times.

After the release of SRBAVG-GEO Edition2D, an error was discovered in the computation of the declination angle and earth-sun distance factor. The angle and factor were computed at 00:00 GMT instead of 12:00 GMT, which is appropriate for computing the solar incoming in local time. This has no effect on the annual mean insolation but significantly affects the monthly zonal solar incoming fluxes near the poles. This error is corrected in the final adjusted TOA fluxes and will also be rectified in the next SRBAVG version (Edition3).

Adjustments to total solar irradiance associated with the spherical Earth assumption are applied zonally to improve the accuracy of incoming solar radiation at each latitude. While these adjustments are applied at the zonal level, the globally averaged correction is the same as in Section 5.1. Similarly, adjustments in SW TOA fluxes due to near-terminator flux biases are also applied zonally without modifying the global mean. Separate adjustments are made for clear and all-sky TOA fluxes.

6.0 References

The full version of CERES EBAF Ed2.6 is available from the following ordering site:
http://ceres.larc.nasa.gov/order_data.php

Doelling et al., 2011: Geostationary enhanced temporal interpolation for CERES flux products. *J. Appl. Meteor. and Clim.*, (submitted).

Fröhlich, C., and J. Lean (1998): The Sun's total irradiance: Cycles, trends and related climate change uncertainties since 1976, *Geophys. Res. Lett.*, 25(23), 4377-4380.

Hansen, J. et al. Earth's energy imbalance: confirmation and implications. *Science* **308**, 1431–1435 (2005).

Kato, S., and N. G. Loeb, 2003: Twilight irradiance reflected by the earth estimated from Clouds and the Earth's Radiant Energy System (CERES) measurements. *Journal of Climate*, 16, 2646–2650.

Kato, S., and N. G. Loeb, 2005: Top-of-atmosphere shortwave broadband observed radiance and estimated irradiance over polar regions from Clouds and the Earth's Radiant Energy System (CERES) instruments on Terra. *J. Geophys. Res.*, 110, doi:10.1029/2004JD005308.

Kopp, G. and Lawrence, G.: "The Total Irradiance Monitor (TIM): Instrument; Design," *Solar Physics*, 230, 1, Aug. 2005, pp. 91-109.

Loeb, N. G., K. J. Priestley, D. P. Kratz, E. B. Geier, R. N. Green, B. A. Wielicki, P. O. R. Hinton, and S. K. Nolan, 2001: Determination of unfiltered radiances from the Clouds and the Earth's Radiant Energy System (CERES) instrument. *J. Appl. Meteor.*, 40, 822–835.

Loeb, N. G., S. Kato, and B. A. Wielicki, 2002: Defining top-of-atmosphere flux reference level for Earth Radiation Budget studies, *Journal of Climate*, 15, 3301-3309.

Loeb, N. G., N. M. Smith, S. Kato, W. F. Miller, S. K. Gupta, P. Minnis, and B. A. Wielicki, 2003: Angular distribution models for top-of-atmosphere radiative flux estimation from the Clouds and the Earth's Radiant Energy System instrument on the Tropical Rainfall Measuring Mission Satellite. Part I: Methodology. *J. Appl. Meteor.*, **42**, 240–265.

Loeb, N. G., S. Kato, K. Loukachine, and N. M. Smith, 2005: Angular distribution models for top-of-atmosphere radiative flux estimation from the Clouds and the Earth's Radiant Energy System instrument on the Terra satellite. Part I: Methodology. *J. Atmos. Oceanic Technol.*, **22**, 338–351.

Loeb, N. G., W. Sun, W. F. Miller, K. Loukachine, and R. Davies, 2006: Fusion of CERES, MISR and MODIS measurements for top-of-atmosphere radiative flux validation, *J. Geophys. Res.*, 111, D18209, doi:10.1029/2006JD007146.

Loeb, N. G., B. A. Wielicki, W. Su, K. Loukachine, W. Sun, T. Wong, K. J. Priestley, G. Matthews, W. F. Miller, and R. Davies, 2007: Multi-instrument comparison of top-of-atmosphere reflected solar radiation, *J. Climate*, **20**, No. 3, 575-591.

Loeb, N. G., B. A. Wielicki, D. R. Doelling, G. L. Smith, D. F. Keyes, S. Kato, N. Manlo-Smith, T. Wong, 2009: Toward Optimal Closure of the Earth's TOA Radiation Budget, *Journal of Climate*, 22, pg 748-766, DOI:10.1175/2008JCLI2637.1.

Loeb, N. G., J. M. Lyman, G. C. Johnson, R. P. Allan, D. R. Doelling, T. Wong, B. J. Soden, G. L. Stephens, 2011a: Observing Changes in Earth's Energy Budget During the Past Decade. *Nature Geosc*. (accepted).

Loeb, N. G., S. Kato, W. Su, T. Wong, F. G. Rose, D. R. Doelling, and J. Norris, 2011b: Advances in understanding top-of-atmosphere radiation variability from satellite observations. *Surveys Geophys*. (submitted).

Lyman, J. M., and G. C. Johnson, 2008: Estimating annual global upper-ocean heat content anomalies despite irregular in situ ocean sampling. *Journal of Climate* 21, 5629–5641.

Minnis P., S. Sun-Mack, D. F. Young, P. W. Heck, D. P. Garber, Y. Chen, D. A. Spangenberg, R. F. Arduini, Q. Z. Trepte, W. L. Smith, Jr., J. K. Ayers, S. C. Gibson, W. F. Miller, V. Chakrapani, Y. Takano, K.-N. Liou, Y. Xie, 2011: CERES Edition-2 cloud property retrievals using TRMM VIRS and Terra and Aqua MODIS data, Part I: Algorithms, *IEEE Trans. Geosci. and Rem. Sens*. (in press).

Purkey, S. G., and G. C. Johnson, 2010: Warming of global abyssal and deep southern ocean waters between the 1990s and 2000s: contributions to global heat and sea level rise budgets. *Journal of Climate* **23**, 6336–6351.

Roemmich, D. et al. Argo: the challenge of continuing 10 years of progress. *Oceanography* **22**, 46–55 (2009).

Sohn, B.-J., J. Schmetz, R. Stuhlmann, and J.-Y. Lee, 2006: Dry bias in satellite-derived clear-sky water vapor and its contribution to longwave cloud radiative forcing. *Journal of Climate*, 19, 5570-5580.

Sun, W., N. G. Loeb, S. Kato, B. Lin, Y. Hu, and C. Lukashin, 2011: A study of subvisual clouds and their radiation effect with a synergy of CERES, MODIS, CALIPSO, AIRS, and AMSR-E data. *Atmos. Chem. Phys*. (submitted).

Thomas S., K. J. Priestley, N. Manalo-Smith, N. G. Loeb, P. C. Hess, M. Shankar, D. R. Walikainen, Z. P. Szewcyzk, R. S. Wilson, D. L. Cooper, 2010: Characterization of the Clouds and the Earth's Radiant Energy System (CERES) sensors on the Terra and Aqua spacecraft, *Proc. SPIE*, Earth Observing Systems XV, Vol. 7807, 780702, August 2010.

Trenberth, K. E., 2009: An imperative for climate change planning: tracking Earth's global energy. Current Opinion in Environmental Sustainability **1**, 19–27.

7.0 Expected Reprocessing

There is no scheduled reprocessing of the CERES EBAF product. However, when there is a reprocessing it will be available for subsetting/visualization/ordering at: http://ceres.larc.nasa.gov/order_data.php.

8.0 Attribution

When referring to the CERES EBAF product, please include the data set version, and the data product. Depending upon what mission is considered, these data sets may be referred to as "CERES EBAF_Ed2.6".

The CERES Team has gone to considerable trouble to remove major errors and to verify the quality and accuracy of this data. Please provide a reference to the following paper when you publish scientific results with the

CERES EBAF_Ed2.6

Loeb, N. G., B. A. Wielicki, D. R. Doelling, G. L. Smith, D. F. Keyes, S. Kato, N. Manlo-Smith, T. Wong, 2009, Toward Optimal Closure of the Earth's TOA Radiation Budget, *Journal of Climate*, 22, pg 748-766, DOI:10.1175/2008JCLI2637.1.

When CERES data are obtained via the CERES web site are used in a publication, we request the following acknowledgment be included: "These data were obtained from the NASA Langley Research Center CERES ordering tool at (http://ceres.larc.nasa.gov/)."

9.0 Feedback and Questions

For questions or comments on the CERES Quality Summary, contact the User and Data Services staff at the Atmospheric Science Data Center. For questions about the CERES subsetting/visualization/ordering tool at http://ceres.larc.nasa.gov/order_data.php, please click on the feedback link on the left-hand banner.